# A Precise and Fast Temperature Mapping Using Water Proton Chemical Shift

Yasutoshi Ishihara, Arturo Calderon, Hidehiro Watanabe, Kazuya Okamoto, Yoshinori Suzuki, Kagayaki Kuroda, Yutaka Suzuki

**A new temperature measurement procedure using phase mapping was developed that makes use of the temperature dependence of the water proton chemical shift. Highly accurate and fast measurements were obtained during phantom and *in vivo* experiments. In the pure water phantom experiments, an accuracy of more than ± 0.5°C was obtained within a few seconds/slice using a field echo pulse sequence (*TR/TE* = 115/13 ms, matrix = 128 × 128, number of slices = 5). The temperature dependence of the water proton chemical shift was found to be almost the same for different materials with a chemical composition similar to living tissues (water, glucide, protein). Using this method, the temperature change inside a cat's brain was obtained with an accuracy of more than ± 1°C and an in-plane resolution of 0.6 × 0.6 mm. The temperature measurement error was affected by several factors in the living system ($B_0$ shifts caused by position shifts of the sample, blood flow, etc.), the position shift effect being the most serious.**

**Key words: temperature mapping; water proton chemical shift; temperature dependence; phase mapping.**

## INTRODUCTION

Mapping the temperature distribution inside a body enables the diagnosis of disorders such as blood circulation and metabolic abnormalities, because body temperature is closely related to physiological functions. Recently, breast cancer and arterial stenosis of the extremities were diagnosed by observing the temperature distribution and the temperature recovery process of the region of interest after heating or cooling the body (1–3). The efficacy of temperature mapping for evaluating myocardial ischemia using intraoperative cardiothermography has been reported (4–6), and it has also been pointed out that body temperature should be monitored during and after cardiac surgery to assure that proper temperature regulation is occurring and to predict low cardiac output syndrome (7). In addition, noninvasive temperature monitoring during hyperthermia (8), other thermotherapies using higher temperatures than hyperthermia, and nonincisional surgery using focused ultrasound (9, 10) and laser treatments (11) is highly desirable for confirming the heating regions and heating efficiency.

**MRM 34:814–823 (1995)**

From Toshiba R & D Center, Kawasaki, 210 Japan (Y.I., A.C., H.W., K.O., Y.S.); Faculty of Engineering, Osaka City University, Osaka, 558 Japan (K. K., Y. S.)

Address correspondence to: Yasutoshi Ishihara, Toshiba R & D Center, 1, Komukai Toshiba-cho, Saiwai-ku, Kawasaki, 210 Japan.

Received February 27, 1995; revised June 22, 1995; accepted June 27, 1995.

0740-3194/95 $3.00



Most NMR parameters such as the equilibrium magnetization $M_0$ (12, 13), the spin-lattice relaxation time $T_1$ (13–20), and the spin-spin relaxation time $T_2$ (13, 14) exhibit temperature dependence. In most cases, however, it is difficult to measure accurately the inner body temperature using only these parameters, because it is difficult to measure their values separately, and the temperature dependence of each parameter varies from organ to organ and tissue to tissue (15, 19, 20).

Recently, noninvasive temperature mapping using the molecular diffusion coefficient D of water was reported (21–25). This method has shown good results with phantom experiments, giving temperature measurements with an accuracy of ± 0.2°C, a spatial resolution of 0.5–1.0 cm, and data acquisition times of 2–5 min (23, 24). However, multiple measurements are necessary to determine D, which extends the measurement time. Moreover, the accuracy of this method seems to be poor in the case of living systems, because the temperature dependence of D is greatly affected by the tissue activation energies (which vary with temperature (25)) and by such tissue conditions as denaturation (26). *In vivo* measurements require the knowledge of these activation energy values for every tissue of interest.

As with D, it is well known that the pure water proton chemical shift is proportional to the temperature (about −0.01 ppm/°C) (27–31). This temperature dependence has been interpreted as resulting from the rupture (27–29), stretching, or a small amount of bending of the hydrogen bonds (29, 30). It has been shown that the temperature distribution can be measured from changes in the water proton chemical shift with temperature (32). It is difficult, however, to detect these changes with high accuracy because the temperature dependent coefficient is small and only large temperature differences can be observed qualitatively.

We have demonstrated that temperature mapping based on three-dimensional magnetic resonance spectroscopic imaging (3D-MRSI) and a spectral estimation method improves the temperature resolution (33, 34). We have also verified that the temperature dependence of the water proton chemical shift for different tissues *in vitro* is almost the same as for pure water (35). This specific temperature dependence means that no calibration curves for each tissue are needed. As another advantage, there is the possibility of measuring the absolute temperature using the chemical shift differences between water and fat (which has no hydrogen bonding) (34). This means that the magnetic field homogeneity and volume susceptibility changes with temperature (36) can be compensated using the fat chemical shift as an inner temperature reference. The disadvantages are poor spatial and temporal resolutions.

To overcome the poor spatial and temporal resolutions, we proposed a fast and precise temperature mapping method based on such chemical shift properties (37) that makes use of phase mapping (38). Comparisons between the numerical simulations of the thermal process and the experimental results have shown that this method is superior to the diffusion method (39). In this paper, we evaluate the accuracy of this technique using phantom experiments and confirm the temperature dependence of the water proton chemical shift differences between individual materials with chemical composition similar to living tissue. The possibility of mapping accurately the inner body temperature distribution is demonstrated by imaging that of a cat's brain. Previously, only qualitative images of human muscle had been obtained (40). We also point out in this paper that the magnetic field changes caused by a position shift of the subject can seriously degrade the temperature accuracy, especially in regions of the large field inhomogeneity.

## PRINCIPLE

It is generally assumed that the water proton chemical shift to lower frequencies with higher temperatures is caused by rupture, stretching or a small amount of bending of the hydrogen bonds (27–30). This means a reduction in the average degree of association of the water molecules, and hence that these shifts are evidence of an increased average shielding constant of the protons. This proton chemical shift change with temperature is thought to be caused by the observed variations of the magnetic field inhomogeneity. In fact, the local magnetic field inhomogeneity $\Delta B_0$ can be represented as the sum of the field inhomogeneity $\delta B_0$ and the chemical shift field caused by magnetic shielding effects Bc, which depends on the temperature distribution $T(\Re)$.

$$\Delta B_O(T(\Re)) = \delta B_O(\Re) + Bc(T(\Re)) \quad [1]$$

in which $\Re$ represents a spatial vector. The inhomogeneity of the magnet and the magnetic susceptibility of the sample produce $\delta B_0$. It must be canceled out to measure the variations of the chemical shift field $\Delta Bc$ with temperature only, for which it is assumed that $\delta B_0$ does not change with temperature for diamagnetic materials. These variations can be calculated by subtracting the field distribution $\Delta B_0(T_0(\Re))$ at a reference temperature $T_0$ from the field distribution $\Delta B_0(T(\Re))$ after a change in temperature. We obtain, then, the field distribution difference as a function of the temperature distribution difference $\Delta T(\Re)$.

$$\begin{aligned} \Delta Bc(\Delta T(\Re)) &= Bc(T(\Re)) - Bc(T_O(\Re)) \\ &= \Delta B_O(T(\Re)) - \Delta B_O(T_O(\Re)) \end{aligned} \quad [2]$$

Such field inhomogeneities can be calculated from the phase image $\theta(\Re)$ obtained with the phase mapping method using the pulse sequence shown in Fig. 1 (38). The time difference $\tau$ between the 90 to 180 degree pulse time $t_1$ and the 180 degree pulse to spin echo time $t_2$ encodes the field distribution as the phase value:

$$\theta(T(\Re)) = \gamma \Delta B_O(T(\Re))\, \tau \quad [3]$$

where $\gamma$ is the gyromagnetic ratio. The temperature distribution can then be calculated using the following equations that subtract the phase distribution at a reference temperature from that after a change in temperature:

$$\begin{aligned} \Delta T(\Re) &= [T(\Re) - T_O(\Re)] \\ &= \Delta Bc(\Delta T(\Re))/\alpha\, B_O \\ &= \Delta\theta(T(\Re))/\alpha\, \gamma\, \tau\, B_O \\ &= [\theta(T(\Re)) - \theta(T_O(\Re))]/\alpha\, \gamma\, \tau\, B_O \end{aligned} \quad [4]$$

where $\alpha$ is the temperature dependent coefficient of the water proton chemical shift expressed in ppm/°C. It is well known that $\alpha$ for pure water is about −0.01 ppm/°C (27, 29, 30).

The temporal resolution obtained with a field echo pulse sequence is superior to that obtained with a spin echo pulse sequence. In this case, $\tau$ is equivalent to the echo time *TE* of the field echo pulse sequence.

## METHODS

### Accuracy of This Method

All the temperature mapping experiments were performed using a 4.7 T MRI system (Toshiba, Kawasaki, Japan) with a 300-mm magnet bore. The measurement error was evaluated with phantom experiments. A spherical phantom ($\phi$ 40 mm) filled with a 1% NaCl solution with dielectric constant and electric conductivity similar to biological tissue at 200 MHz was fixed to a quadrature type probe ($\phi$ 120 mm). First, to evaluate how the measurement error is affected by system instabilities caused by shim current drifts, the transceiver radio frequency, the superconductive current, and noise, phase images were obtained with the field echo pulse sequence every 10 min for 2 h (*TR*/*TE* = 115/13 ms, matrix size = 128 × 128, FOV = 85 × 85 mm, number of slices = 5, and slice thickness = 3 mm), after 5 h of positioning the phantom and turning on the system. The four 5 × 5-pixel regions of interest (ROI) were chosen to evaluate the measurement error and detect any error distributions.

Second, to obtain the phase images with temperature changes and to evaluate the measurement error, the

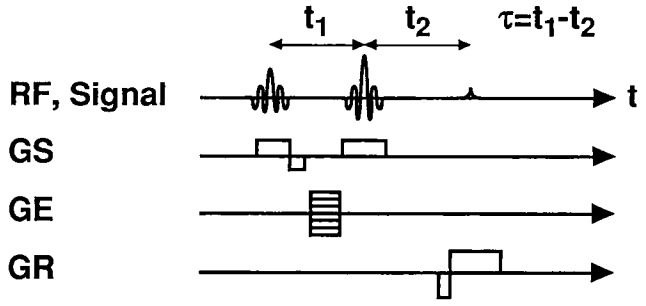


FIG. 1. Phase mapping pulse sequence.

phantom was subjected to inductive heating using a continuous wave at 200 MHz and 10 W. The measurement error was estimated using the temperature obtained with a copper-constantan thermocouple placed near the center of the phantom. Phase mapping with the field echo pulse sequence using the above-mentioned sequence parameters was carried out to obtain the phase images. In this experiment, horizontal measurement planes were selected. The phase images inside the phantom were then measured every minute during the cooling process. The phase differences at each temperature were calculated by subtracting from these images the phase image at the reference temperature before heating. To estimate the accuracy, the temperature dependence of the water proton chemical shift of this solution had to be determined using these different phase distributions. A ROI neighboring the thermocouple was chosen to remove the thermal inhomogeneities caused by the inductive heating, and the mean phase value in the ROI was obtained to remove the dispersion in the phase images due to noise. The chemical shift changes obtained from the phase value in the ROI were compared with the temperatures measured by the thermocouple.

### Temperature Dependencies of the Water Proton Chemical Shift for Individual Tissues

The temperature dependencies of the water proton chemical shift for different tissues were evaluated using materials similar in chemical composition to biological tissue. Agar and the white of an egg were chosen as a glucide and a protein, respectively. Each material was enclosed in a spherical glass container and degassed by aspirating and boiling to suppress the growth of bubbles during heating. Each sample was solidified by cooling it after placing a thermocouple at its center. The temperature of the samples was controlled by inductive heating. The phase images were measured and processed with the procedures mentioned above. In addition, the temperature dependence in chicken muscle was also evaluated. In this case, the chicken muscle was wrapped in thin vinyl film to prevent evaporation by heating. The temperature dependencies for individual materials were obtained from the mean phase value in the ROI neighboring the thermocouple plotted against the temperatures measured by the thermocouple.

### *In vivo* Imaging of the Internal Temperature Changes

To confirm the feasibility of imaging a body's internal temperatures, anesthetized and immobilized cats were used for *in vivo* experiments. The whole body was heated with hot air at about 10°C above the surrounding temperature, or only the head was heated up to 40°C by inductive heating using the same heating procedure as for the phantom. The brain temperature changes were imaged and measured with thermocouples set under the dura mater. Body temperature was measured with a thermocouple in the rectum. Temperature changes during the cooling process were also measured.

## RESULTS

The phase measurement errors during the 2-h interval obtained after 5 h of turning on the system are shown in Fig. 2, where the mean values and standard deviations of the phase differences in the four ROIs in the central measurement plane have been plotted. The phase drifts of the mean values were within the range −3.8–+4.8 °C, which is less than the ± 5°C range corresponding to the worst case using a pure water temperature dependent coefficient. The measurement errors were interpreted as being produced mainly by magnetic field drifts and image noise, corresponding to the mean value drifts and standard deviations in Fig. 2, respectively, considering that the surrounding temperature changes were less than 0.2°C during imaging.

The experiment to confirm the temperature imaging accuracy of this method was carried out next. The inner temperature increased about 10°C from an initial temperature $T_0$ of 35°C after heating the 1% NaCl solution phantom for 10 minutes. The phase difference images in the central plane at each temperature ($\Delta T$ = 4°C, 8°C, 12°C, 16°C) are shown in Fig. 3. In this paper, the signs of the calculated phase differences and chemical shift changes have been inverted to have brighter image intensities correspond to higher temperatures. The phase changes are proportional to temperature changes. The temperature dependent coefficient of this solution was calculated from the relationship between the average phase value in the ROI near the thermocouple at the phantom's center and the temperatures measured by the thermocouple. This relationship is shown in Fig. 4. The reason for averaging the phase values and selecting such a ROI is that each phase distribution was almost homogeneous at the center of the phantom, whereas the temperature distributions at the edge were less homogeneous because of heat transportation by radiation. The result in

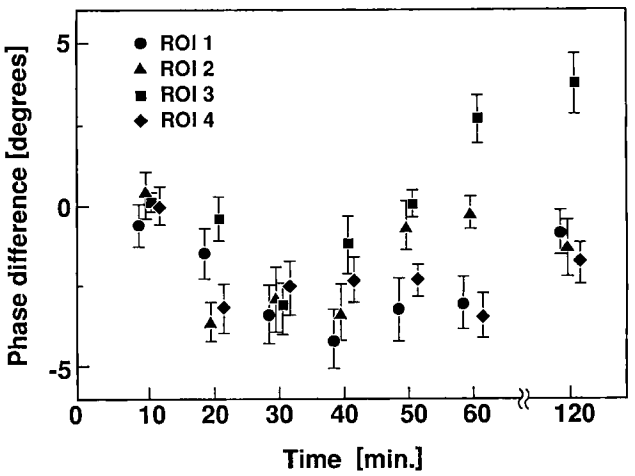


FIG. 2. Phase measurement errors caused by system instabilities during a 2-h interval obtained 5 h after positioning the solution phantom and turning on the system. The phase images were obtained with a field echo pulse sequence every 10 min. Each point represents the phase difference calculated by subtracting from each image the corresponding phase of the first image and averaging the values in the four ROIs in the central measurement plane.

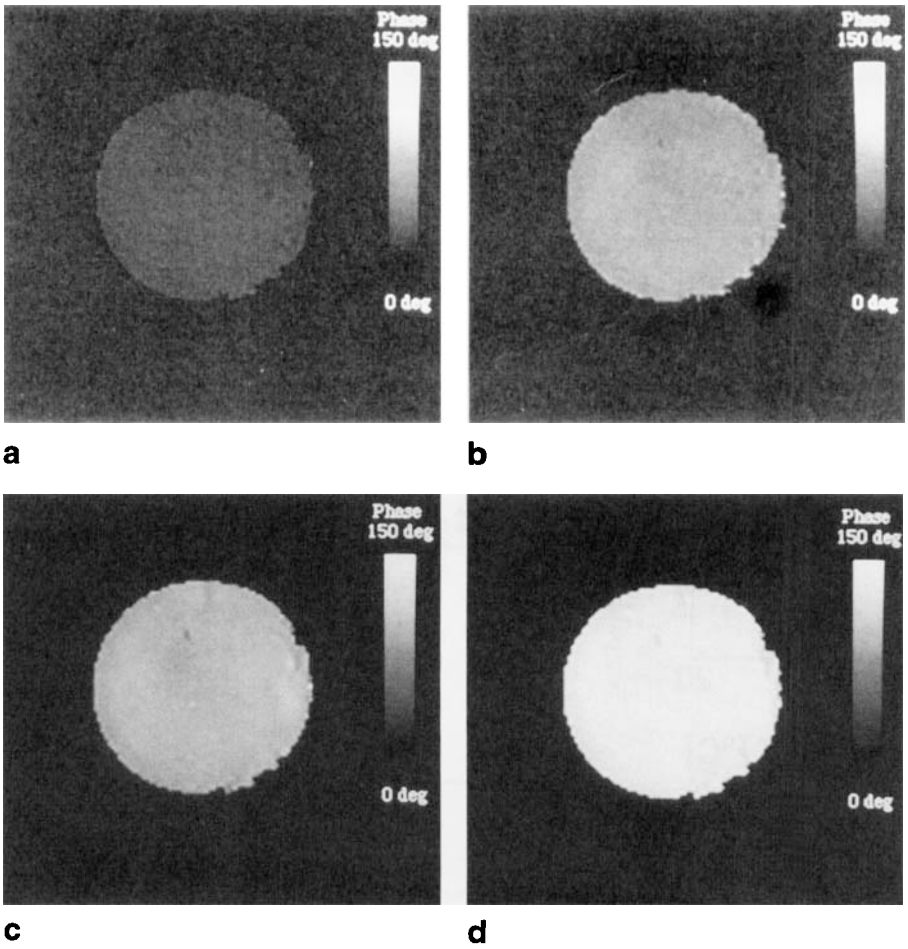


FIG. 3. Phase maps of the 1% NaCl solution phantom at different temperatures. The phase differences in images (a), (b), (c), and (d) reflect temperature changes $\Delta T$ of 4°C, 8°C, 12°C, and 16°C from the reference temperature $T_0$ of 35°C. The temperature changes were controlled using inductive heating with a continuous wave at 200 MHz and 10 W, and the temperature was measured using copper-constantan thermocouples.

Fig. 4 gives a temperature dependent coefficient for the phase of 8.82 degree/°C, corresponding to the coefficient of a water proton chemical shift of −0.0098 ppm/°C. The standard deviation of the observed phase at each temperature was less than 1.5 degrees (corresponding to about ± 0.17°C) and the correlation coefficient was 0.999.

The temperature dependencies of the water proton chemical shift for various materials are shown in Fig. 5 and summarized in Table 1. Individual temperature dependencies were almost the same, although the phase deviation measured at each temperature was larger and the correlation coefficients were slightly smaller for the agar, the white of an egg and chicken muscle than for the 1% NaCl solution. The reasons for these larger deviations seemed to be an inhomogeneous heating effect and local magnetic inhomogeneities caused by the bubbles produced during heating. Although larger, these deviations were less than 0.003 ppm and too small to include in the figure.

Figure 6 shows the estimated temperature error for each material calculated by subtracting the expected value obtained using the average temperature dependent coefficient of all the materials (−0.010 ppm/°C) from the measured value at each temperature change. These errors consisted of the difference of the mean values and standard deviations mainly involving the effects caused by the magnetic field drifts and the image noise shown in Fig. 2, and the temperature dependence differences. The deviations caused by only the differences in the temperature dependence were estimated to be less than 0.5°C, even if the temperature changes exceeded 10°C.

In the whole body heating experiment, the brain temperature was raised to 37°C from an initial temperature $T_0$ of 35°C. Figure 7 shows axial phase images of a cat's head (Fig. 7a) at different temperatures. The images in Figs. 7b, 7c and 7d reflect temperature changes $\Delta T$ of 0.4°C, 0.8°C and 1.2°C from the reference temperature $T_0$ of 35°C measured with the thermocouple set under the dura mater. In the head heating experiment, the brain temperature was raised to 38°C. Figure 8 shows phase images similar to those in Fig. 7. The images in Figs. 7a, 7b, 7c and 7d reflect temperature changes $\Delta T$ of 0.6°C, 1.2°C, 1.8°C and 2.4°C from the reference temperature $T_0$ of 35°C. Although it is desirable to heat the subject homogeneously to obtain accurate measurement errors (e.g., with an extracorporeal bypass method), Fig. 7 and Fig. 8 confirm that a heating distribution with acceptable homogeneity was obtained in the center of the brain. Figure 9 shows the chemical shift changes with temperature calculated using the mean phase value in the ROI near the thermocouple (Fig. 7a). The temperature dependent coefficient of the water proton chemical shift and the correlation coefficient were −0.0093 ± 0.0006 ppm/°C and 0.932 for the whole body heating experiment. Those for the head heating experiment were −0.0106 ± 0.0006 ppm/°C and 0.953.

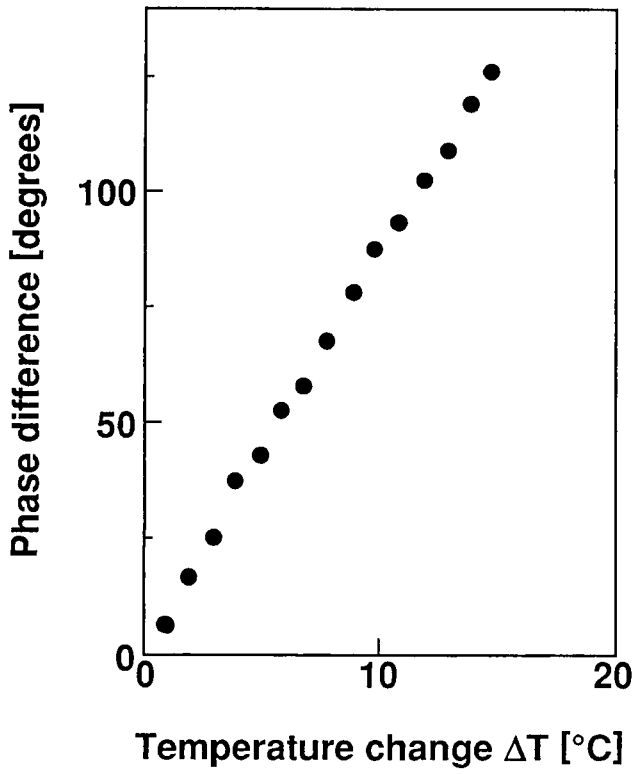


FIG. 4. Temperature dependence of the water proton chemical shift of a 1% NaCl solution. The temperature changes were measured with a thermocouple, and the phase differences were calculated from the average phase values surrounding the thermocouple.

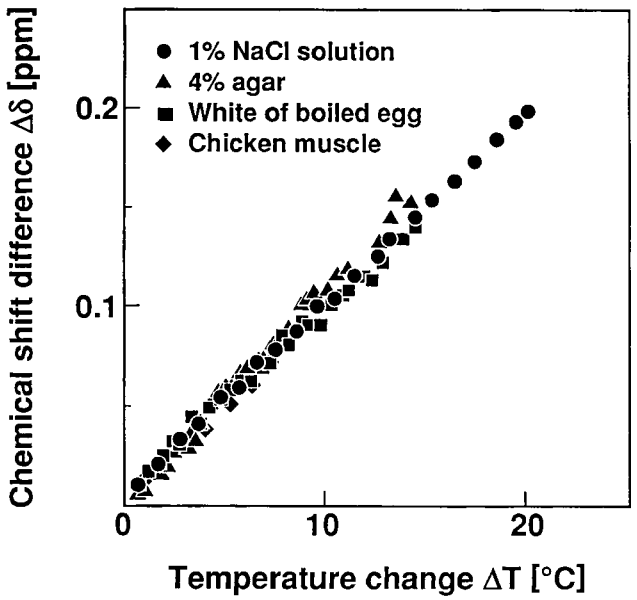


FIG. 5. Temperature dependence of the water proton chemical shift estimated for individual materials similar to living tissue and chicken muscle. The vertical axis shows the chemical shift differences obtained from the phase values using eq. [3]. The deviations were too small to be included. The temperature dependence values are summarized in Table 1.

Table 1
Temperature Dependence of Individual Samples

| Object | Temperature dependence [ppm/°C] | Correlation coefficient |
|---|---|---|
| 1% NaCl solution | 0.0098 ± 0.0003 | 0.999 |
| 4% agar | 0.0103 ± 0.0006 | 0.997 |
| White of boiled egg | 0.0091 ± 0.0006 | 0.996 |
| Chicken muscle | 0.0114 ± 0.0006 | 0.987 |

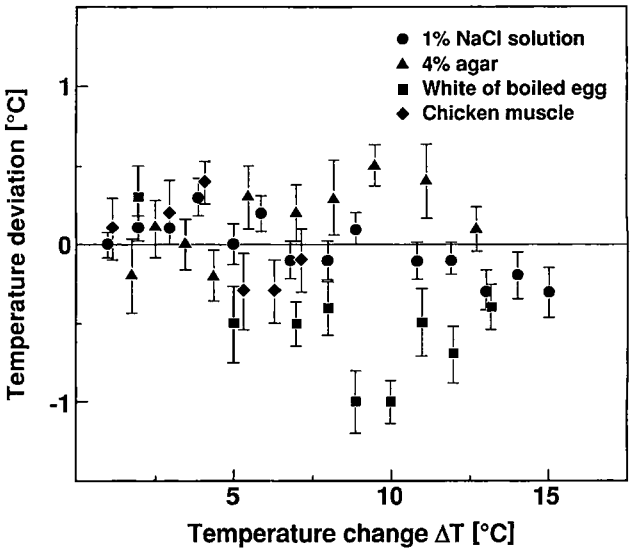


FIG. 6. Temperature measurement errors for individual materials. These errors were obtained by subtracting the expected value obtained using the average temperature dependence (−0.010 ppm/°C) from the measured value at each temperature change.

The measurement errors surrounding the brain area observed in Fig. 7 and Fig. 8 corresponded to field inhomogeneity changes produced by movements of the cat's head (Fig. 10). These phase images were acquired every 30 min without temperature changes. The regions near the edge of the brain and the eyeballs were especially affected by these movements.

## DISCUSSION

The advantages of this method have attracted the attention of some researchers (36, 39–43), but there has been almost no discussion of the temperature dependence of materials similar to these in a living system and the error of this method.

The measurement error of the experiments (< 1°C) was seen to be affected mainly by four parameters: magnetic field drifts caused by system instabilities, image noise, temperature dependence differences between individual materials, and susceptibility changes with temperature.

Figure 2 was interpreted as the measurement error affected by image noise and magnetic field drifts caused by system instabilities. This was verified by observing that the temperature changes in the region surrounding the phantom (less than 0.2°C) had no effect on the measurement error. In fact, the temperature near the thermocouple was homogeneous (also less than 0.2°C).

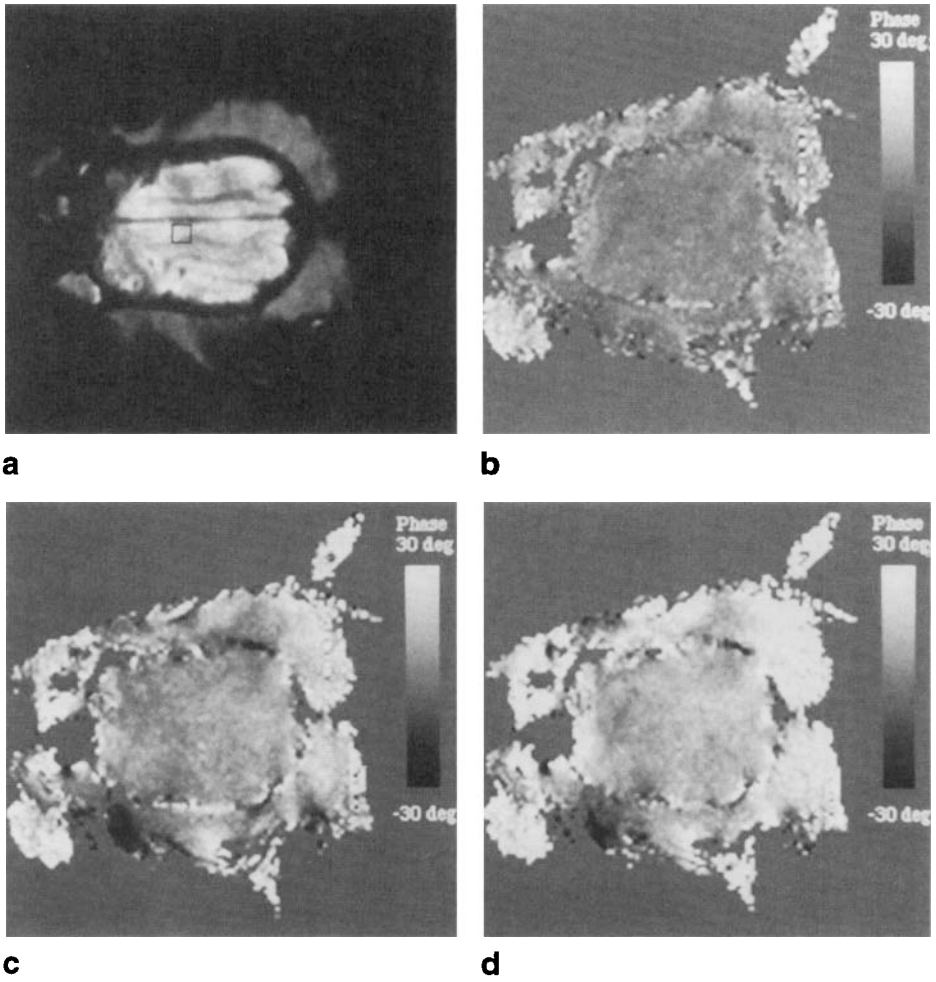


FIG. 7. Phase maps at different temperatures obtained from a cat's head in the axial plane (a) under whole body heating using hot air at about 10°C above the ambient temperature. The phase differences in (b), (c), and (d) reflect temperature changes $\Delta T$ of 0.4°C, 0.8°C, and 1.2°C from the reference temperature $T_0$ of 35°C.

The origin of the change of the mean phase values in Fig. 2 was considered to be the magnetic field drifts. Magnetic field drifts or fluctuations of 0.01 ppm will give a phase change corresponding to a 1°C temperature measurement error. There are several reasons for these magnetic field drifts (e.g., shim currents and transceiver frequency drifts). Slight thermal expansions of the shim coils caused by the shim currents may also generate magnetic field drifts immediately after the system is turned on. Although it was confirmed that typical long-term drifts were less than 0.001 ppm/h in our system, measurement errors seemed to result from the short-term fluctuations caused by the above-mentioned factors, which determine the intrinsic accuracy of the system. This effect was seen to be less than ± 0.5°C from the result in Fig. 2.

On the other hand, the standard deviations of the phase for each measurement shown in Fig. 2 were considered to be caused by image noise. The errors caused by these phase deviations are approximately given by $\mathrm{Tan}^{-1}[1/(S/N)]$ (S/N being the image signal to noise ratio). In this experiment, image noise produced a phase deviation of about 5 degrees, in agreement with the results in Fig. 2. A spatial resolution lower than 0.66 × 0.66 × 3 mm would lead to more accurate temperature measurements if we consider the temperature distribution to vary gradually. In this case, the $T_2$* effect inside a voxel was taken into consideration to determine the optimum voxel size.

The differences in the temperature dependent coefficients of the water proton chemical shifts between different tissue types generate measurement errors. The differences were less than 0.0023 ppm/°C with the materials used in our experiments (Table 1), which generated a measurement error of less than ± 0.5°C within a 10°C range using the average temperature dependent coefficient (−0.010 ppm/°C) instead of calibration curves for individual materials. The temperature changes during a study or a diagnosis are usually within the 30–40°C range, producing a measurement error of less than 0.5°C. Although these differences produce about a 2.5°C measurement error for a 50°C temperature change during cancer therapy using higher temperature heating, it is considered a reasonable value for confirming the heating region and heating efficiency. The total error involving these factors in the phantom experiment was estimated to be less than ± 1°C (Fig. 6).

The similarity between the temperature dependent coefficient for the brain tissue and those for the 1% NaCl solution, agar, white of an egg and chicken muscle was verified with the results of the cat experiment (Fig. 9), although the controlled temperature range was smaller. It seems possible, then, to map the temperature difference distribution with higher accuracy using the average tem-

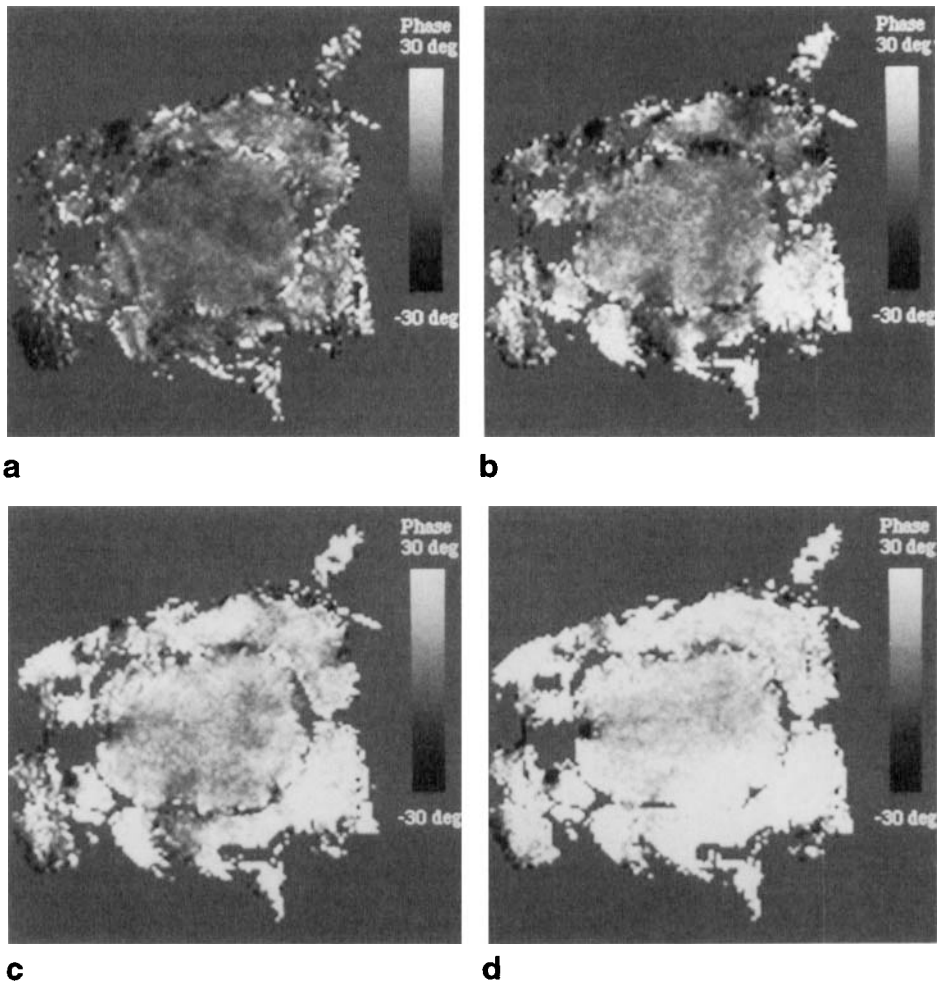


FIG. 8. Phase maps at different temperatures obtained from a cat's head after heating it using inductive heating. The phase shift differences in (a), (b), (c) and (d) reflect temperature changes ΔT of 0.6°C, 1.2°C, 1.8°C, and 2.4°C from the reference temperature $T_0$ of 35°C. The measurement plane is the same as in Fig. 7a.

perature dependence (−0.010 ppm/°C) than with other temperature mapping methods ($T_1$, $T_2$, D). It is necessary, however, to confirm the temperature dependence for all tissues and under such conditions as denaturation to measure the temperature distributions precisely. For our *in vivo* experiments, inasmuch as it was not possible to insert the thermocouple into the cat's brain too deeply and to heat the cat excessively, it was essential to have good agreement between the measurement plane and the thermocouple's position, as well as wide range temperature control.

In addition, magnetic field drifts caused by such factors as position shifts of the subject, have to be considered during *in vivo* experiments. Figure 10 shows how position shifts influence the phase error. Position shifts of the cat tend to affect the regions with large field inhomogeneities in the first image (e.g., the edge of the brain and near the eyeballs). The measurement errors surrounding the brain area in Fig. 7 and Fig. 8 are attributed to this problem. However, because the phase errors in the central region were the same as in the phantom case, it seemed that precise temperature changes could be measured in this region in 2 h. To overcome subject movement, it is necessary to detect any internal reference signal that is insensitive to temperature. One solution may be to use the chemical shifts of fat as an internal temperature reference in 3D-MRSI (34).

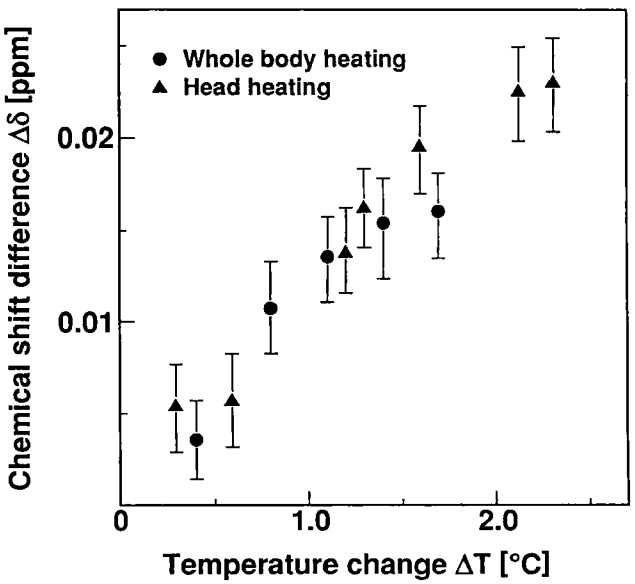


FIG. 9. Temperature dependence of the water proton chemical shift in a cat's brain. The temperature changes were measured with a thermocouple set under the dura mater, and the phase differences were calculated from the average phase values inside the central brain ROI in Fig. 7a.

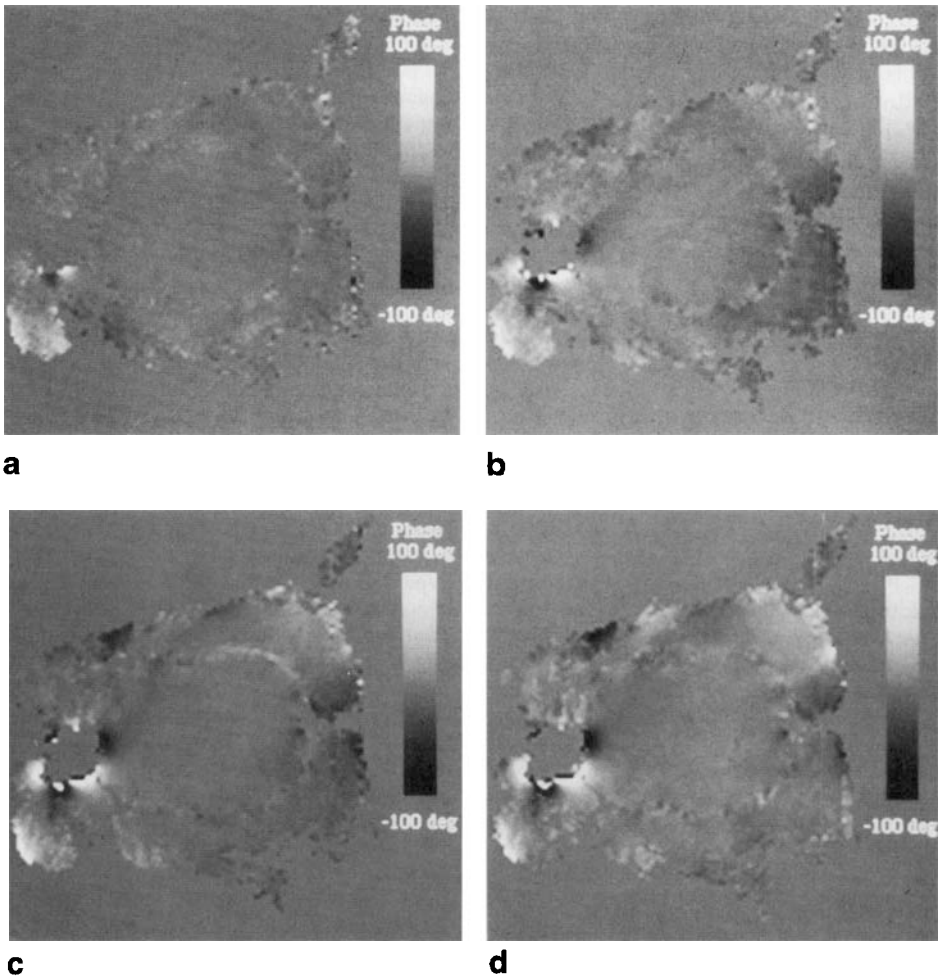


FIG. 10. Effects that position shifts of a cat's head have on the phase error. The images were obtained without temperature changes. Panels (a), (b), (c) and (d) show the phase shift changes after 30 min, 60 min, 90 min, and 120 min.

Blood oxygenation, blood flow, and susceptibility changes with temperature should also be considered in the living system. Although the susceptibility of paramagnetic species varies with temperature according to Curie's law, this effect does not seem to be serious for normal tissues with homogeneous susceptibility distributions. If volume susceptibility changes occur due to tissue oxygenation changes with temperature such as those observed in functional MRI where an activation task gives rise to a local increase in (cortical) neuronal activity (44), they produce field inhomogeneity changes and consequently induce temperature measurement errors. However, there is also the possibility of compensating the magnetic field changes, including susceptibility changes with temperature, using the chemical shift differences between water and fat, because these changes induce both water and fat chemical shift changes in a voxel. This means that it may be necessary to combine both methods (phase mapping and 3D-MRSI) to overcome this effect. Blood flow changes with temperature generate a phase error when perfusion at the capillary level in a voxel has an average direction. The perfusion effects on the measurement error must be evaluated in the future.

All our experiments were made with a 4.7 T MRI system. Such a high field has two advantages. One is good S/N, which reduces the measurement time or the voxel size; a by-product of small voxel sizes is avoiding decreased signal intensities due to susceptibility effects in the voxel. Another advantage is that higher fields give the same phase change with shorter *TE*s, which leads to shorter *TR*s and total acquisition times, because higher fields convert the certain chemical shift change into a larger phase change with the same *TE*. Hence, we must choose the voxel size and *TE* based on the field strength, acquisition time and accuracy.

## CONCLUSIONS

A new temperature measurement procedure using phase mapping gives highly accurate and fast measurements. This method could be used to map the body's internal temperature distribution with high accuracy because the temperature dependence of the water proton chemical shift is independent of tissue type. This could be especially useful when monitoring body temperature during cancer treatment with high power heating (> 80°C) using ultrasound or laser. The accuracy of the temperature measurements in this case was predicted to be about 2.5°C. It could also be very useful and effective during and after operations for the early detection of hemodynamic disturbances. In addition, if the relationship between the disorder and recovery processes after heating or cooling the body is understood, it will be possible to

diagnose abnormalities with this method by detecting the deviations from normal temperature greater than 1°C.

Future work will evaluate the effects of such factors as magnetic susceptibility and blood flow change on the temperature dependence of the water proton chemical shift in living systems. Furthermore, because the acquisition time for the phase mapping sequence can be decreased using fast imaging techniques such as echo planar imaging, real-time body temperature monitoring may become feasible in the future.

## ACKNOWLEDGMENTS

The authors thank Dr. Kaoru Itoh (Department of Neurosurgery, Tokai University) for his help in performing the animal experiments.

## REFERENCES

1. M. M. Raskin, M. M. Lopez, J. J. Sheldon, Lumbar thermography in discogenic disease. *Radiology* **119,** 149–152 (1976).
2. J. M. Spitalier, D. Giraud, F. Amalric, The importance of the abnormal and isolated breast thermogram. *Acta Thermogr.* **5,** 152 (1980).
3. R. Pochaczevsky, C. E. Wexler, P. H. Meyers, J. A. Epstein, J. A. Marc, Liquid crystal thermography of the spine and extremities. *J. Neurosurg.* **56,** 386–395 (1982).
4. J. Senyk, A. Malm, S. Bornmyr, Intraoperative cardiothermography. *Eur. Surg. Res.* **3,** 1–12 (1971).
5. F. Robicsek, T. N. Masters, R. H. Svenson, W. G. Daniel, Experimental observation of coronary blood flow using the thermographic camera. *Coll. Works Cardiopulm. Dis.* **22,** 57–64 (1979).
6. W. Daniel, H. Klein, R. Hetzer, Thermocardiography—a method for continuous assessment of myocardial perfusion dynamics in the exposed animal and human heart. *Thorac. Cardiovasc. Surg.* **27,** 51–57 (1979).
7. H. R. Matthews, J. B. Meade, C. C. Evans, Peripheral vasoconstriction after open-heart surgery. *Thorax* **29,** 338–342 (1974).
8. J. H. Kim, E. W. Hahn, Clinical and biological studies of localized hyperthermia. *Cancer Res.* **39,** 2258–2261 (1979).
9. H. E. Cline, J. F. Schenck, R. D. Watkins, K. Hynenen, F. A. Jolesz, Magnetic resonance-guided thermal surgery. *Magn. Reson. Med.* **30,** 98–106 (1993).
10. H. E. Cline, K. Hynenen, C. J. Hardy, R. Watkins, J. F. Schenck, F. A. Jolesz, MR temperature mapping of focused ultrasound surgery. *Magn. Reson. Med.* **31,** 628–636 (1994).
11. V. D. Köchli, C. A. v. Weymarn, K. Zweifel, J. D'Alfonso, G. K. v. Schulthess, Towards monitoring percutaneous laser discectomy with temperature sensitive echo planar imaging, *in* "Proc., SMRM, 12th Annual Meeting, New York, 1993," p. 157.
12. Y. Amemiya, Y. Kamimura, Thermometry of hot spot using NMR for hyperthermia. *Trans. IECE* **J66-C,** 203–210 (1983).
13. B. Knüttel, H. P. Juretschke, Temperature measurements by nuclear magnetic resonance and its possible use as a means of *in vivo* noninvasive temperature measurement and for hyperthermia treatment assessment. *Recent Results Cancer Res.* **101,** 109–118 (1986).
14. J. L. Ackerman, L. C. Clark Jr, S. R. Thomas, R. G. Pratt, R. A. Kinsey, F. Becattini, NMR thermal imaging, *in* "Proc., SMRM, 3rd Annual Meeting, New York, 1984," p. 1–2.
15. B. D. Youl, C. P. Hawkins, J. K. Morris, E. P. G. H. DuBoulay, P. S. Tofts, *In vivo* $T_1$ values from guinea pig brain depend on body temperature. *Magn. Reson. Med.* **24,** 170–173 (1992).
16. I. R. Young, J. W. Hand, A. Oatridge, M. V. Prior, N. Saeed, G. R. Forse, Impact of perfusion changes on *in vivo* measurement of temperature with MRI using $T_1$ changes, *in* "Proc., SMRM, 12th Annual Meeting, New York, 1993," p. 1279.
17. J. H. Simpson, H. Y. Carr, Diffusion and nuclear spin relaxation in water. *Phys. Rev.* **111,** 1201–1202 (1958).
18. D. L. Parker, V. Smith, P. Sheldon, L. E. Crooks, L. Fussell, Temperature distribution measurements in two-dimensional NMR imaging. *Med. Phys.* **10,** 321–325 (1983).
19. R. J. Dickinson, A. S. Hall, A. J. Hind, I. R. Young, Measurement of changes in tissue temperature using MR imaging. *J. Comput. Assist. Tomogr.* **10,** 468–472 (1986).
20. A. S. Hall, M. V. Prior, J. W. Hand, I. R. Young, R. J. Dickinson, Observation by MR imaging of *in vivo* temperature changes induced by radio frequency hyperthermia. *J. Comput. Assist. Tomogr.* **14,** 430–436 (1990).
21. D. LeBihan, J. Delannoy, R. L. Levin, Mapping of temperature using intra-voxel incoherent motion (IVIM) MR imaging application to hyperthermia, *in* "Proc., SMRM, 7th Annual Meeting, San Francisco, 1988", p. 881.
22. D. LeBihan, J. Delannoy, R. L. Levin, Temperature mapping with MR imaging of molecular diffusion: application to hyperthermia. *Radiology* **171,** 853–857 (1989).
23. J. Delannoy, C. N. Chen, R. Turner, R. L. Levin, D. LeBihan, Noninvasive temperature imaging using diffusion MRI. *Magn. Reson. Med.* **19,** 333–339 (1991).
24. Y. Zhang, T. V. Samulsky, W. T. Joines, J. Mattiello, R. L. Levin, D. LeBihan, On the accuracy of noninvasive thermometry using molecular diffusion magnetic resonance imaging. *Int. J. Hyperthermia* **8,** 263–274 (1992).
25. L. A. Woolf, Tracer diffusion of tritiated water (THO) in ordinary water ($H_2O$) under pressure. *J. Chem. Soc. Faraday I.* **71,** 784–796 (1975).
26. D. LeBihan, J. Delannoy, R. Levin, J. Pekar, O. LeDour, Temperature dependence of water molecular diffusion in brain tissue., *in* "Proc., SMRM, 8th Annual Meeting, Amsterdam, 1989," p. 141.
27. W. G. Schneider, H. J. Bernstein, J. A. Pople, Proton magnetic resonance chemical shift of free (gaseous) and associated (liquid) hydride molecules. *J. Chem. Phys.* **28,** 601–607 (1958).
28. N. Muller, Concerning structural models for water and chemical-shift data. *J. Chem. Phys.* **43,** 2555–2556 (1965).
29. J. C. Hindman, Proton resonance shift of water in the gas and liquid states. *J. Chem. Phys.* **44,** 4582–4592 (1966).
30. N. Muller, R. C. Reiter, Temperature dependence of chemical shifts of protons in hydrogen bonds. *J. Chem. Phys.* **42,** 3265–3269 (1965).
31. N. W. Lutz, A. C. Kuesel, W. E. Hull, A $^1$H-NMR method for determining temperature in cell culture perfusion systems. *Magn. Reson. Med.* **29,** 113–118 (1993).
32. L. D. Hall, S. L. Talagara, Mapping of pH and temperature distribution using chemical-shift-resolved tomography. *J. Magn. Reson.* **65,** 501–505 (1985).
33. K. Kuroda, N. Somatani, Y. Suzuki, Y. Ishihara, K. Okamoto, Y. Suzuki, Temperature mapping using water proton chemical shift., *in* "Proc., SMR, 2nd Annual Meeting, San Francisco, 1994," p. 1569.
34. K. Kuroda, Y. Suzuki, Y. Ishihara, K. Okamoto, Y. Suzuki, Temperature mapping by water proton resonance frequency obtained with 3D-MRSI. *Magn. Reson. Med.*, in press.
35. K. Kuroda, Y. Miki, N. Nakagawa, S. Tsutsumi, Y. Ishihara, Y. Suzuki, K. Sato, Non-invasive temperature measurement by means of NMR parameters—Use of proton chemical shift with spectral estimation technique. *Med. Biol. Eng. Comput.*

**29,** 902 (1991).
36. J. De Poorter, The proton resonance frequency method for noninvasive MRI thermometry: study of susceptibility effects., *in* "Proc., SMR, 2nd Annual Meeting, San Francisco, 1994," p. 426.
37. Y. Ishihara, A. Calderon, H. Watanabe, K. Mori, K. Okamoto, Y. Suzuki, K. Sato, K. Kuroda, N. Nakagawa, S. Tsutsumi, A precise and fast temperature mapping using water proton chemical shift, *in* "Proc., SMRM, 11th Annual Meeting, Berlin, 1992," p. 4803.
38. K. Sekihara, S. Matsui, H. Kohno, A new method of measuring static field distribution using modified Fourier NMR imaging. *J. Phys. E.* **18,** 224–227 (1985).
39. J. De Poorter, C. De Wagter, Y. De Deene, C. Thomsen, F. Ståhlberg, E. Achten, The proton-resonance-frequency-shift method compared with molecular diffusion for quantitative measurement of two-dimensional time-dependent temperature distribution in a phantom. *J. Magn. Reson.* **103,** 234–241 (1994).
40. J. De Poorter, C. De Wagter, Y. De Deene, C. Thomsen, F. Ståhlberg, E. Achten, Non-invasive *in-vivo* thermometry with the proton resonance frequency method: qualitative results in human muscle, *in* "Proc., SMRM, 12th Annual Meeting, New York, 1993," p. 738.
41. R. Stollberger, M. Fan, E. Ebner, P. W. Ascher, R. Kleinert, Mapping of temperature changes in heterogeneous tissues for the monitoring of hyperthermia, *in* "Proc., SMRM, 12th Annual Meeting, New York, 1993," p. 156.
42. J. R. MacFall, T. V. Samulski, D. M. Prescott, E. Fullar, Thermal mapping using the MR image phase *in vivo* during hyperthermia, *in* "Proc., SMR, 2nd Annual Meeting, San Francisco, 1994," p. 1578.
43. R. Stollberger, E. Ebner, P. W. Ascher, Real-time temperature imaging of interstitial laser thermotherapy using the water proton chemical shift, *in* "Proc., SMR, 2nd Annual Meeting, San Francisco, 1994," p. 1584.
44. K. K. Kwong, J. W. Belliveau, D. A. Chesler, I. E. Goldberg, C. E. Stern, J. R. Baker, R. M. Weisskoff, R. Benson, B. P. Poncelet, B. E. Hoppel, D. N. Kennedy, R. Turner, M. S. Cohen, T. J. Brady, B. R. Rosen, Real time imaging of perfusion change and blood oxygenation change with EPI, *in* "Proc., SMRM, 11th Annual Meeting, Berlin, 1992," p. 301.